Proceedings of the International Conference on Heat Exchanger Fouling and Cleaning - 2024 (Peer-reviewed)
April 21–26, 2024, Lisbon, Portugal; Editors: H.U. Zettler and E.M. Ishiyama

DESIGN AND CHARACTERISATION OF A THIN PLATE HEAT EXCHANGER FOR FOULING STUDIES

***J. Brown[1], S.M. Clarke[2], G. Kawaley[3], M.J. Sargent[2], M. Turner[2] and D.I. Wilson[1]**
[1] Department of Chemical Engineering and Biotechnology, Philippa Fawcett Drive, University of Cambridge, CB3 0AS, UK, jr606@cam.ac.uk
[2] Institute for Energy and Environmental Flows, University of Cambridge, Madingley Rise, CB3 0EZ, UK
[3] Mitsubishi Electric R&D Centre Europe B.V., 17 Firth Road, Livingston, EH54 5DJ, UK

ABSTRACT

A well-designed apparatus for fouling studies will allow different types of data to be collected simultaneously, reproducibly, under quantified flow, thermal and chemical conditions. The development and application of a thin plate heat exchanger for testing fouling in liquids and liquid solutions is reported. The device operates under constant temperature driving force, with heat transferred across a 1 mm thick × 12 mm wide and 150 mm long test section. The test liquid flows through a long rectangular duct with one heated wall section, and deposition can be monitored visually as well as quantified from heat transfer measurements. The thermal performance of the device is characterised in terms of hot and cold duties as well as local surface temperature measurements employing thermochromic liquid crystalline coatings. The data are compared with a coupled computational fluid dynamics and heat transfer simulation, which also estimates the rate of heat loss to ambient. These show reasonably good agreement. Application of the device to fouling studies is demonstrated using aqueous solutions of calcium sulphate. Uneven deposit distribution is observed, however, which complicates interpretation of the results.

INTRODUCTION

Fouling is the reduction in heat transfer performance resulting from build-up of deposits or soiling layers with poor thermal conductivity on heat transfer surfaces. Fouling can be mitigated or avoided by understanding how deposition occurs, and the contributions from factors such as temperature, rates of transport of heat, mass and momentum, as well as the nature and form of the heat transfer surface. In some cases, these can be manipulated by design or operating strategies in order to avoid fouling; in others, they can be optimised to reduce the rate of fouling or enhance the efficiency of cleaning.

A number of experimental devices have been developed for laboratory studies of fouling, some of which mimic operating geometries and conditions closely while others employ more ideal configurations to allow more information to be collected from each fouling run. The latter provide fundamental insights into mechanisms which can be transferred to other systems and incorporated into simulations to either design or predict the performance of heat exchangers. For fouling driven by high surface temperature, the devices can be classified as those operating at constant heat flux – usually provided by electrical heating - or those operating at fixed temperature driving force – readily achieved by circulating cold and hot utilities at constant temperature.

Devices can then be further classified as those with well defined fluid flow patterns (most commonly in rectangular ducts with a heated wall [1,2]; inside heated cylinders or pipes [3-6]; on the inner surface of an annular test section; [7, 8]. These often require pumping circuits and significant volumes of test liquids (we concentrate on liquid phase fouling). Where small batches of fluid are available or batch size needs to be minimised, heated fouling probes immersed in an agitated volume are frequently used [9-12]. One of the reasons why systems with well-defined flows are used is the need for reliable estimates of local surface temperatures, mass transfer rates and local shear stresses, so that variations in fouling behaviour or deposit coverage can be attributed to these parameters or to other factors in the fouling mechanism. Modern computational fluid dynamics (CFD) modelling can, ostensibly, provide this for more complex flow geometries but verification is still required and the computational resource can be high.

An additional classification is access to the deposit for inspection or further study (*e.g.* for cleaning studies). Systems with detachable or removable test sections are then highly desirable (*e.g.* [1], [2], [3], [12]) and certain geometries favour these. Flat test surfaces allow standard surface

ISBN: 978-0-9984188-3-4; Published online www.heatexchanger-fouling.com

profilometers to be used to map deposit coverage, and many surface analysis techniques are designed for flat samples.

A final mode of classification (beyond the engineering aspects of the temperatures, pressures and nature of fluids to be handled in the experiments) is the scope for changing the nature of the heat transfer surface to be tested. Coatings, as well as modified and structured surfaces have received much attention in the fouling community (*e.g.* [2]) and fabrication or preparation of test surfaces at the prototype stage is more straightforward for certain geometries.

This paper reports the development and application of a thin plate heat transfer and fouling apparatus. The plate forms the heated wall of a long rectangular duct and allows deposition to be monitored visually as well as via heat transfer measurements. The surface can be coated or modified as desired, and samples can be readily removed and subjected to a range of analytical techniques. The apparatus approximates constant wall temperature condition by using co-current operation and the process fluid can be heated or cooled. The heat transfer performance of the apparatus is characterised using fluid temperature measurements and CFD simulations. Heat losses to ambient are also estimated using the simulations. The plate surface temperature was measured using thermochromic liquid crystal coatings.

The apparatus has been used for studies of calcium sulphate and calcium carbonate fouling at solution temperatures up to 80°C. The ease of plate removal from the fouling cell allows for structural characterisation of deposits.

RIG DESCRIPTION

Figure 1 shows a diagram and a photograph of the apparatus. The main flow loop starts from a stirred 4-L jacketed glass vessel, which serves as a reservoir where the test solution can be heated or cooled. Liquid passes through a centrifugal pump and rotameter before entering the long rectangular duct of the heat transfer cell. The main body of the cell is made of polyethyletherketone (PEEK, a polymer with high mechanical strength and poor conductivity compared to metal) while the front cover is clear polycarbonate, allowing visualisation of the flow channel. The duct is 12 mm wide and its height can be reduced from 12 mm to 1 mm by the use of polycarbonate inserts. The inserts allow a wide range of velocities (and Reynolds numbers, *Re*) to be studied without changing the pump. Heat is transferred across a thin metal plate in the section of established flow in the duct, following a 26 cm entry length. The dimensions of the heat transfer area, *A*, are 12 mm × 140 mm with semi-circular ends, giving $A = 1650$ mm^2. The metal plate is up to 1 mm thick and is held in place by a 4 mm thick brass block. The plate can be readily removed for examination or modification.

The utility fluid is supplied from a heater/circulator and flows through an adjacent rectangular duct. Heat transfer and fouling tests have been conducted with the two fluids flowing upwards in a co-current arrangement in order to achieve a more uniform surface temperature distribution and to deter bubbles from adhering to the walls.

The inlet and outlet temperatures of each fluid are measured using Pt100 temperature sensors (uncertainty ± 0.03°C). Experiments are performed at constant flow rate, measured using rotameters (± 0.05 L min^{-1}), and constant temperature driving force. Chemical monitoring, such as pH and conductivity, is performed using electrodes in contact with the liquid in the reservoir.

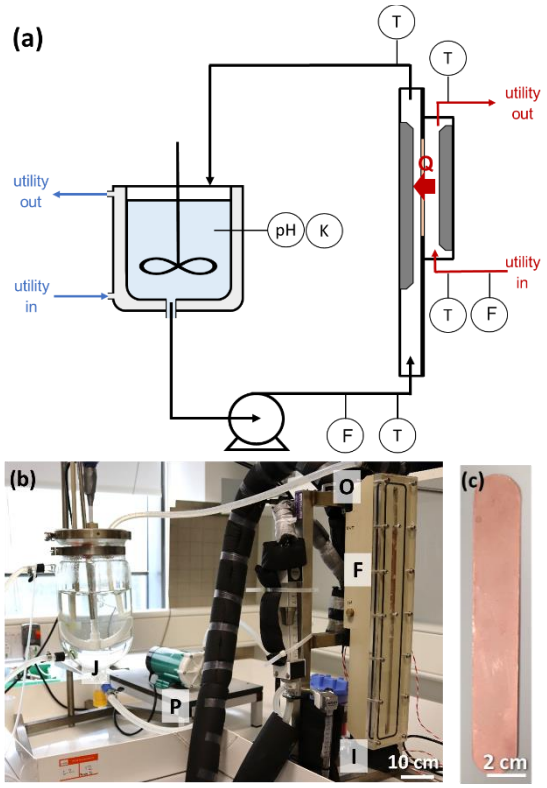

Figure 1. (*a*) Diagram and (*b*) photograph of the duct heat transfer cell experimental setup; (*c*) thin copper plate insert. J – jacketed reservoir; P – centrifugal pump; F – fouling cell; I – cell inlet; O – cell outlet.

HEAT TRANSFER CHARACTERISATION

Heat Balance

The thermal performance of the duct flow cell was characterised by comparing the duties for the two fluids. For these tests, the process solution was deionised water, initially at room temperature, and the utility fluid was an aqueous 20% v/v propylene glycol solution. The temperature sensors and the flow meters were calibrated and the rig was insulated. The magnitude of the duty, *Q*, for each fluid was calculated from:

ISBN: 978-0-9984188-3-4; Published online www.heatexchanger-fouling.com

$$Q = \dot{m} C_p |T_{in} - T_{out}| \quad (1)$$

where $\dot{m}$ is the mass flow rate, C_p is the constant pressure heat capacity and T_{in} and T_{out} are the inlet and outlet temperatures, respectively. The difference in Q between the two fluids was found to depend on both the flow rates and temperatures: lower flow rates and higher temperatures resulted in greater losses to the environment, *i.e.* $Q_{\text{hot stream}} > Q_{\text{cold stream}}$. The average difference for the flow rates and temperatures employed in the fouling runs was 8%.

Surface Temperature

It is highly desirable to know the temperature at the surface of the metal plate for modelling the crystallisation fouling process. Inserting thermocouples into the plate was not an option due to its slenderness, so thin thermochromic liquid crystal coatings (TLCs) were employed, similar to those reported by Besevic *et al.* [12]. The coating thickness, measured using a confocal thickness scanner, was 100 µm. In their microencapsulated form, TLCs exhibit a degree of water resistance for a number of hours, depending on shear rate. R35C01W coatings from SpotSee/Hallcrest, UK, were applied to sample plates. These coatings start to change from black to red at 35.0°C. The transition temperature was verified by attaching fast response thermocouples to the coated plates and heating them in air. The observed colours and the associated temperatures are displayed in Fig. 2.

The thermal conductivity of the coating, according to the supplier, lies in the range 0.2 – 0.4 W $m^{-1}K^{-1}$, giving a thermal resistance of 2.5-5×10^{-4} m^2 K W^{-1}. For comparison, the thermal resistance of the copper plate was 2.5×10^{-6} m^2 K W^{-1}; the measured film heat transfer coefficients were of order 2-3 kW $m^{-2}K^{-1}$, corresponding to thermal resistances of 3.3-5×10^{-4} m^2 K W^{-1}.

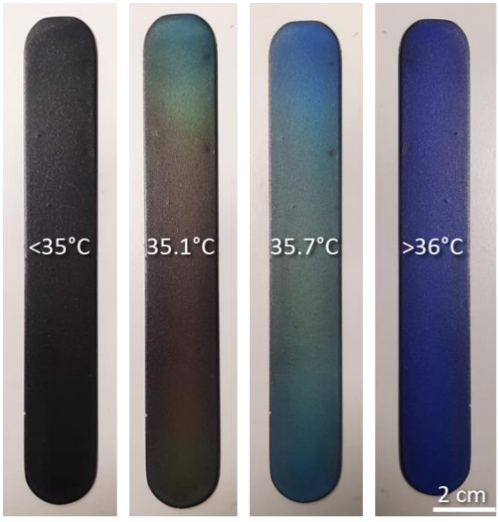

Figure 2. Colour change of TLC-coated copper plates. The temperatures labelled were measured in the middle of the plate.

The surface temperature was evaluated for a range of cold-side flow rates, with the same hot-side (utility) flow rate of 8.2 L min^{-1}. The jacketed vessel maintained the cold-side inlet temperature at 20°C. The hot side temperature was increased in 0.5 K intervals until the coating colour changed.

The average cold-side convective heat transfer coefficient, h_c, could then be determined for a given flow rate based on the measured Q (Eqn. (1)), plate surface temperature, T_s, given by the TLCs, and cold temperature T_c, taken as the arithmetic average of T_{in} and T_{out} for the cold fluid:

$$h_c = \frac{Q/A}{(T_s - T_c)} \quad (2)$$

The Nusselt number, *Nu*, was calculated using the hydraulic diameter of the duct, d_H, and water thermal conductivity, k_c:

$$Nu = \frac{h_c d_H}{k_c} \quad (3)$$

The Prandtl number, *Pr*, was calculated from:

$$Pr = \frac{\mu_c C_p}{k_c} \quad (4)$$

where μ_c is the water dynamic viscosity. The Reynolds number, *Re*, was determined using

$$Re = \frac{F \rho_c d_H}{A_{xs} \mu_c} \quad (5)$$

where ρ_c is the density of the cold fluid, F is the volumetric flow rate, and A_{xs} is the cross-sectional area of the rectangular duct.

Fouling Runs

The fouling runs reported here were conducted with supersaturated aqueous solutions of calcium sulphate, with inlet temperatures of 90°C and 50°C. These temperatures correspond to conditions in modern heat pumps such as those employed in the heating, refrigeration and air conditioning (HVAC) sector. Experiments to date have been performed with copper (C106) plates, while further experiments are planned with stainless steel and modified surfaces. Copper is commonly used in this sector owing to its high thermal conductivity.

Calcium sulphate ($CaSO_4$) solutions were prepared using equimolar quantities of calcium nitrate tetrahydrate ($Ca(NO_3)_2 \cdot 4H_2O$) and sodium sulphate (Na_2SO_4), both of which are very soluble in water. In the presence of a heated surface, calcium sulphate dihydrate (gypsum, $CaSO_4 \cdot 2H_2O$) is expected to crystallise due to its inverse-solubility behaviour. The counter-ions remaining, Na^+ and NO_3^-, are both associated with high, normal solubility behaviour. The chemical equilibrium is

$$Ca(NO_3)_2 \cdot 4H_2O_{(s)} + Na_2SO_{4\,(s)} \leftrightarrow CaSO_4 \cdot 2H_2O_{(s)} + 2NaNO_{3\,(aq)} + 2H_2O_{(l)} \quad (6)$$

Each of the precursor chemicals was dissolved separately in hot deionised water and then added

ISBN: 978-0-9984188-3-4; Published online www.heatexchanger-fouling.com

slowly to preheated deionised water in the jacketed vessel. The resulting solution contained 24.6 mmol L^{-1} of $CaSO_4$, giving a 140% saturation at the bulk temperature of 50°C.

The fouling solution was circulated through the flow loop at 1.5 L min^{-1} ($Re \approx 5{,}200$ in the duct) with the utility flow rate again at 8 L min^{-1} ($Re \approx 25{,}000$ in its duct). Runs lasted from 24 to 72 hours. The inlet and outlet temperatures of each fluid were logged every minute. Calcium concentration was determined by titration against EDTA on aliquots withdrawn from the jacketed vessel at 2-hourly intervals in the daytime, including at the start and end of each run. The system was operated in batch mode and the components were not topped up during a run.

CFD MODELLING

The mismatch in the heat balance has been investigated using a coupled flow and heat transfer simulation in ANSYS Fluent originally developed for another similar rig. Preliminary results are presented here. Developing a high quality mesh has proved to be challenging and is the subject of ongoing work.

The process and utility flowrates and inlet temperatures were set to those used for the fouling tests. Water was used as the utility fluid instead of the aqueous propylene glycol mixture. The two rigs have approximately the same dimensions: height, flow path length, plate size and depth. The body of the modelled rig is 2.5 cm wider. The largest difference between the CFD model and the experimental rig is the depth of the flow channel: the former is 3 mm and the latter is 6 mm, as this model is only intended to provide preliminary results for heat leakage, but the process side Reynolds numbers are comparable.

Model Description

The symmetry of the rig is exploited to lower the computational requirements. Some key parameters of the simulation are given in Table 1 and the mesh is shown in Figure 3. Tetrahedral elements were used throughout.

Table 1: Key parameters in CFD calculations

Number of elements	17,983,931
Minimum orthogonal quality	0.126
Number of elements in utility fluid flow path	1,106,844
Number of elements in process fluid flow path	9,000,060
Process fluid flow path body sizing	0.2 mm
y^+ process fluid	19.2
Utility fluid flow path body sizing	0.3 mm
y^+ utility fluid	115.6
Turbulence model	Transition SST
Pressure velocity coupling	SIMPLE
Process side Reynolds number	6,600
Utility side Reynolds number	54,000

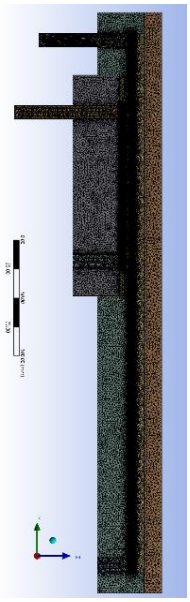

Figure 3. Mesh for CFD simulation.

Table 2 summarises the accuracy of the coupled heat and mass calculations. Mass balance discrepancies were around 0.02% on the utility side and 0.04% on the process side. The calculated heat balance discrepancy was 0.05%.

Table 2. Residuals reached for CFD simulation

Residual quantity	Convergence Level
Continuity	4.2×10^{-2}
Velocity (largest)	9.8×10^{-5}
Energy	8.0×10^{-7}
k	3.4×10^{-4}
ω	2.1×10^{-4}
Intermittency	1.9×10^{-4}
Re_Θ	1.2×10^{-4}

Heat leakage

$Q_{\text{hot stream}}$ is expected to be greater than $Q_{\text{cold stream}}$ owing to losses to ambient. One of the main aims of the CFD study was to establish that the difference in duties was consistent with the expected losses. Thermal energy is expected to flow from the walls of the hot utility duct through the body of the flow cell to ambient. Thermal energy could also flow from the warmed solution into the body of the cell to ambient, thereby reducing the estimate of the enthalpy gained by the fluid according to Eqn. (1).

A typical exterior film heat transfer co-efficient value of h_{ext} = 10 W m^{-2} K^{-1} [13] and a free stream

ISBN: 978-0-9984188-3-4; Published online www.heatexchanger-fouling.com

temperature of 20°C were applied for all exterior surfaces. Fig. 4(*a*) shows the computed temperature distribution across the central plane (also a plane of symmetry). Along the entry length, heat loss to ambient raises the surface temperature to around 303 K (30°C): at the test section, this rises to around 318 K (45°C). This heat is likely to arise from conduction from the heating utility around the process stream duct, through the body walls. Beyond the heat transfer section, the surface temperature returns to around 300 K.

Overall, the simulation predicted an overall heat loss of 9% to the environment, which is comparable to that measured on the experimental rig. The total heat flow from the process fluid to the walls was 1.2 W for the half-section, which is small compared to the net heat gain of the process fluid along the half-cell, of 111 W. These computational results also provide support for studies where the cell is used to study heat transfer in different fluids and the use of structured surfaces.

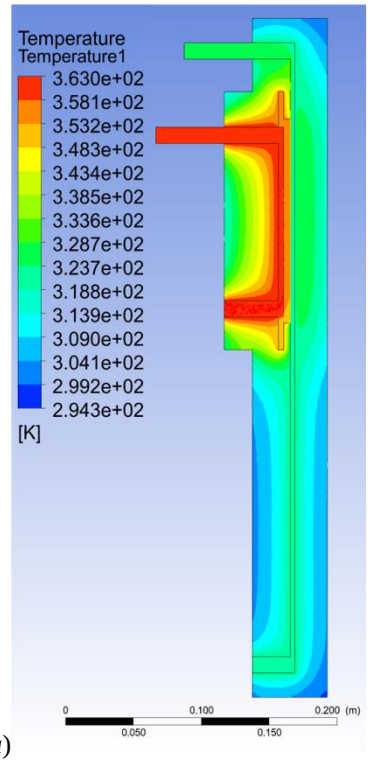

(*a*)

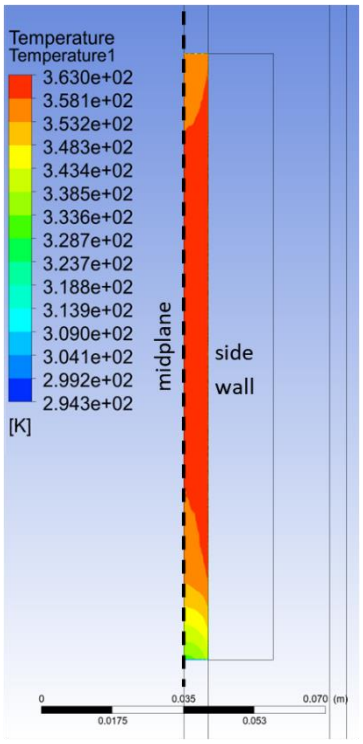

(*b*)

Figure 4. Calculated temperature distribution on the (*a*) central plane of symmetry, and (*b*) half the plate surface in contact with the process stream, for a clean plate. Flow in both liquids is upwards. The inlet temperatures and flowrates were set to be those in the fouling runs: hot side, 8 L min^{-1}, T_{in} 90°C (363 K); cold side, 1.5 L min^{-1}, T_{in} 50°C (323 K). Note different temperature scales.

ISBN: 978-0-9984188-3-4; Published online www.heatexchanger-fouling.com

RESULTS AND DISCUSSION

Plate Surface Temperature

The film heat transfer coefficients for the process fluid, determined directly from TLC measurements, for a range of Reynolds numbers are shown in Figure 5(a). The data collected at 20°C were used to calculate the Nusselt number and are presented in the form of a *Nu*-*Re* correlation in Figure 5(b)). Correction of density, viscosity and thermal conductivity in Eqs (3)-(5) for temperature allowed extrapolation of h_c to higher temperatures, of interest for the fouling studies.

The data are compared to the following correlations in Fig. 5(b).

(*i*) Sieder-Tate, valid in the laminar regime:

$$Nu = 1.86 Re^{1/3} Pr^{1/3} \left(\frac{d_H}{L}\right)^{1/3} \quad (7)$$

Here, L is the length of the heated section.

(*ii*) Dittus-Boelter correlation, turbulent regime. Two dependencies on *Pr* were evaluated:

$$Nu = 0.023 Re^{0.8} Pr^{0.4} \quad (8)$$

$$Nu = 0.023 Re^{0.8} Pr^{0.3} \quad (9)$$

(*iii*) Gnielinski, turbulent regime:

$$Nu = \frac{(C_f/2)(Re-1000)Pr}{1+12.7\sqrt{C_f/2}\left(Pr^{2/3}-1\right)} \quad (10)$$

where C_f is the Fanning friction factor, given by:

$$C_f = 0.079 Re^{-0.25} \quad (11)$$

Inspection of the loci in Fig. 5(b) shows that the data lie within the range of the above correlations. The values at low *Re* are higher than the Sieder-Tate estimates, which is expected as the *Re* values correspond to the transition regime. In an ideal case C_f would be determined from the pressure drop. This was not done here, and the pressure drop due to flow is expected to be small compared to the hydrostatic head.

Fouling Runs

Figure 6(a) shows an example of a fouled copper plate. The deposit coverage is uneven: beyond the initial wake region, the amount of deposit increases towards the upper end of the plate where the process stream is slightly warmer. The surface temperature map in Fig. 4(*b*) indicates that the end regions are expected to feature lower temperatures: at the bottom, owing to the development of the thermal boundary layer and at the top, arising from conduction through the brass block into the cell body. The edges of the flow channel are seen to promote crystal nucleation. The SEM image of the deposit in Fig. 6(*b*) shows prismatic crystals, indicating that the $CaSO_4$ has deposited as gypsum rather than the anhydrous or hemihydrate polymorphs.

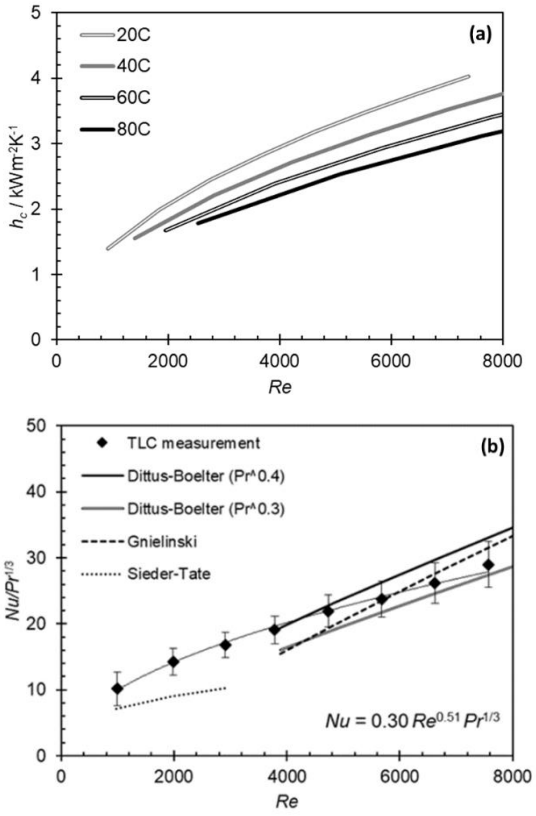

Figure 5. Effect of Reynolds number on cold-side film heat transfer coefficient for a range of temperatures in (*a*) dimensional, and (*b*) dimensionless form. Also plotted on (*b*) are estimates from standard correlations, and the result obtained by fitting the data to a simple power law relationship.

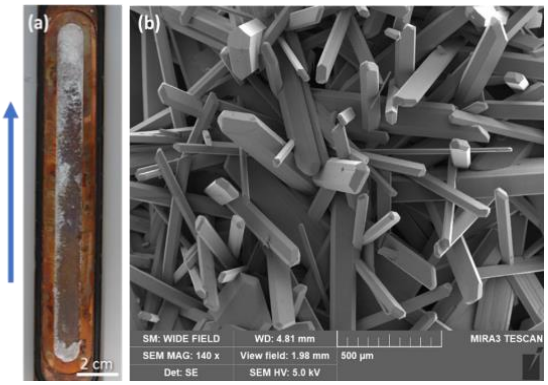

Figure 6. Example of calcium sulphate deposit on copper plate. (*a*) photograph. Arrow indicates flow direction. (*b*) Scanning electron micrograph (SEM) image of the deposit.

Heat transfer data collected during a fouling run are presented in Fig. 7. There is no evident induction period and the overall heat transfer coefficient

ISBN: 978-0-9984188-3-4; Published online www.heatexchanger-fouling.com

decreases steadily over time. The fouling Biot number, Bi_f, was calculated from

$$\frac{U}{U_{clean}} = \frac{1}{1+Bi_f} \quad (12)$$

where U_{clean} is the initial value for a completely clean surface. In this case shown here, R_d approaches a value of 12.5 K m^2 W^{-1} (corresponding to Bi_f =0.4) asymptotically, indicating that fouling had a significant impact on the rate of heat transfer. Under these conditions, of almost constant temperature driving force, the surface temperature of the deposit changes from the clean value of 89.0°C to a final value of 81.0°C.

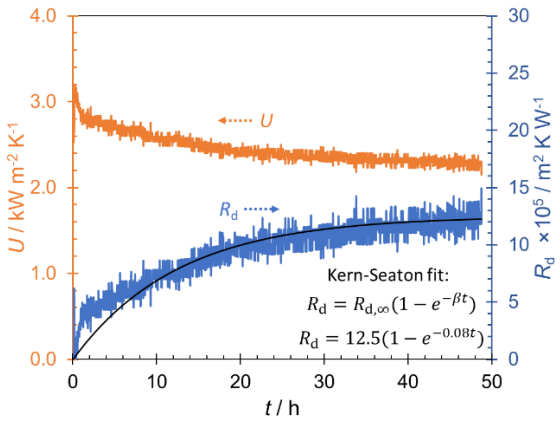

Figure 7. Evolution of the overall heat transfer coefficient, U, and the calculated deposit fouling resistance, R_d, for a $CaSO_4$ fouling run. Inlet temperatures were 90°C (utility) and 50°C (process fluid), $CaSO_4$ concentration 24.6 mmol L^{-1}. Fig. 8 shows the temperature and concentration profiles.

The evolution of R_d follows a trend which can be described reasonably well after t =10 h by the Kern-Seaton model. The approach to steady state ($dR_d/dt = 0$) could result from one or more of the following mechanisms:

(*i*) balance of rate of deposition and rate of removal due to shear, as postulated by Kern and Seaton;

(*ii*) depletion of calcium ions from solution as deposition progresses for this batch system, resulting in [Ca] at the surface reaching the saturation level at the local temperature $[Ca]_{sat}$;

(*iii*) reduction in the temperature of the deposit-solution interface, $T_{deposit}$, which decreases oversaturation and thus deposition driving force and also gives lower rate constants.

The concentration data in Fig. 8 indicate that the solution remained supersaturated with respect to surface temperature throughout the run, which excludes mechanism (*ii*). The estimated deposit interface temperature decreased by around 8 K over the course of the experiment, and a surface temperature of 80°C would still be expected to cause some deposition. Fig. 7 indicates that the rate of change of U does not reach zero, so steady state is not quite reached.

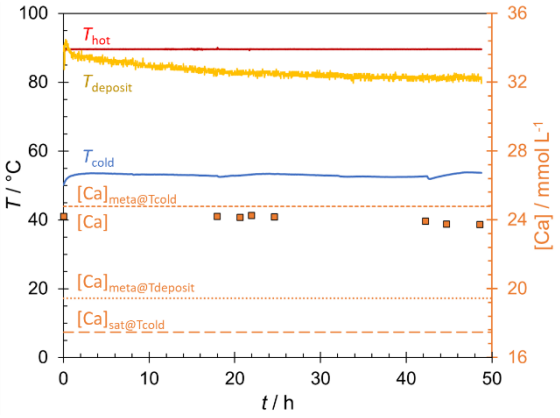

Figure 8. Evolution of temperatures and calcium concentration for the fouling run in Fig. 7. $T_{deposit}$ is the average temperature at the deposit-solution interface, based on measured h_c values and the average instantaneous heat flux (= $Q_{cold\ stream}/A$), estimated using Eqn. (2). The orange squares represent the measured calcium concentration, [Ca]. Horizontal dashed lines indicate the saturation calcium concentration at the bulk solution temperature, T_{cold}, the metastable calcium concentration in the bulk solution $[Ca]_{meta}$, and at $T_{deposit}$.

It is evident from Fig. 6 that the deposition pattern is uneven, with some regions – roughly 50% by area – free of any visually evident foulant, and the deposit coverage heavier towards the exit. This means that the calculated value of U includes contributions from clean regions and heavily fouled ones. The $T_{deposit}$ estimate in Fig. 8 will then overestimate the value in a fouled region as the local heat flux there will be lower than the average value. Accurate estimation of local temperatures is further complicated by the presence of the crystalline deposit, which Fig. 6 indicates will give rise to local roughness effects (which will persist to clean regions nearby). Mechanism (*iii*) cannot, therefore be excluded completely. Schlüter *et al.* [5] considered these variations in calculating local deposit thermal resistances.

Finally, no conclusions can be drawn about mechanism (*i*) because the deposition pattern is uneven and there is no systematic variation with location that is needed for this explanation.

Variation in local surface temperature on the clean heat transfer surface has been investigated using the CFD simulation. The temperature of the plate increases initially as the cold fluid is heated. The plate is cooler at the end compared to the middle as the hot fluid cools.

ISBN: 978-0-9984188-3-4; Published online www.heatexchanger-fouling.com

CONCLUSIONS

The performance of the thin plate heat exchanger fouling cell design has been characterised. The thermochromic liquid crystalline coatings provide useful verification of the thermal performance of the device. The CFD simulation confirmed the expected rate of heat loss through the fouling cell body, and the low rate of heat loss from the test solution. Tests using calcium sulphate solution demonstrate the applicability of the device for studying fouling: the non-uniformity of the deposits is not yet understood and this variation complicates quantitative analysis of the results.

The authors have not registered the design and details are available from the authors if other workers wish to construct similar devices. The thin plate configuration renders it ideal for testing surface coatings, while the visualisation window also supports cleaning studies.

NOMENCLATURE

A	Area, m^2
A_{xs}	Area of duct cross-section, m^2
Bi_f	Fouling Biot number, dimensionless
C_p	Specific heat capacity, J kg^{-1} K^{-1}
C_f	Fanning friction factor, dimensionless
d_H	Hydraulic diameter, m
F	Volumetric flow rate, m^3 s^{-1}
h	Film heat transfer coefficient, W m^{-2} K^{-1}
k	Thermal conductivity, W m^{-1} K^{-1}
L	Length, m
$\dot{m}$	Mass flow rate, kg s^{-1}
Nu	Nusselt number, dimensionless
Pr	Prandtl number, dimensionless
Q	Heat flow, W
R_d	Thermal resistance, K m^2 W^{-1}
Re	Reynolds number, dimensionless
T	Temperature, °C
U	Overall heat transfer co-efficient, W m^{-2} K^{-1}
β	Kern-Seaton fit parameter, s^{-1}
μ	Dynamic viscosity, Pa s
ρ	Density, kg m^{-3}

Subscripts

c	Cold stream
clean	Clean
d	Deposit
ext	Exterior
in	Inlet
out	Outlet
s	Surface
∞	At infinite time

REFERENCES

[1] T.M. Pääkkönen, M. Riihimaki, C.J. Simonson, E. Muurinene, R.L. Keiski, Modeling $CaCO_3$ crystallization fouling on a heat exchanger surface – Definition of fouling layer properties and model parameters, *Intl J. Heat Mass Transfer*, Vol. 83, pp 84-98, 2015.

[2] O.M. Magens, J.F.A. Hofmans, Y. Adriaenssens and D.I. Wilson, Comparison of fouling of raw milk and whey protein solution on stainless steel and fluorocarbon coated sufaces: Effects on fouling performance, deposit structure and composition, *Chem. Eng. Sci*., Vol. 195, pp. 423-432, 2019.

[3] D.I. Wilson and A.P. Watkinson, A study of autoxidation reaction fouling in heat exchangers, *Can. J. Chem. Eng*., Vol. 74, pp. 236-246, 1996.

[4] B.D. Crittenden, S. A. Hout and N. J. Alderman, Model experiments of chemical reaction fouling, *Chem. Eng. Res. Des*., Vol. 65, pp. 165-170, 1987.

[5] F. Schlüter, W. Augustin and S. Scholl, Application of experimental data to model local fouling resistances, *Heat Mass Transfer*, Vol. 58, pp. 29–40, 2022.

[6] R. Goedecke, P. Drögemüller, W. Augustin and S. Scholl, Experiments on integral and local crystallization fouling resistances in a double-pipe heat exchanger with wire matrix inserts, *Heat Transfer Eng*., Vol. 37, pp. 24-31, 2016.

[7] R. Challa, D. Johnston, V. Singh, M. Tumbleson and K. Rausch, Fouling characteristics of model carbohydrate mixtures and their interaction effects, *Food Bioprod. Proc*., Vol. 93, pp. 197-204, 2015.

[8] M. Ghedamu, A.P. Watkinson and N. Epstein, Mitigation of Wax Build-up on Cold Surfaces, *Fouling Mitigation of Industrial Heat Exchange Equipment*, Begell House, NY, pp. 473–489, 1997.

[9] A. Young, S.A. Venditti, C. Berrueco, M. Yang, A. Waters, H. Davies, S. Hill, M. Millan and B.D. Crittenden, Characterisation of crude oils and their fouling deposits using a batch stirred cell system, *Heat Transfer Eng*., Vol. 32, pp. 216-227.

[10] B. Petkovic and A.P. Watkinson, Fouling of a heated rod in a stirrer tank system, *Heat Transfer Eng*, 2014, Vol. 35 (3), pp. 302-310.

[11] E. Davoudi, B. Moghadas and K. Bahareh, Modeling and estimation of fouling factor on the hot wire probe by smart paradigms, *Chem. Eng. Res. Des*., Vol. 188, pp. 81-95, 2022.

[12] P. Besevic, S.M. Clarke, G. Kawaley, and D.I. Wilson, A novel fouling cell to study influence of solution on crystallisation fouling, *Proc. Intl. Conf. Heat Exchanger Fouling and Cleaning 2017*, Madrid, Spain, 2017.

[13] R.L. Shilling, K.J. Bell, P. M. Bernhagen, T.M. Flynn, P.S. Hrnjak, F.C. Standiford, K.D. Timmerhaus, Heat-Transfer Equipment, in *Perry's Chemical Engineers' Handbook*, 7th ed., eds. R.H. Perry, D.W. Green, pp. 11-1–11-118, McGraw-Hill, New York, 1997.

ISBN: 978-0-9984188-3-4; Published online www.heatexchanger-fouling.com